LA-UR-98-2230

Possible Satellite-based Observations of the 1997 Leonid Meteoroids

Morris B. Pongratz, Group NIS-1
Robert C. Carlos, Group NIS-1
Thomas Cayton, Group NIS-2
Los Alamos National Laboratory
Los Alamos, New Mexico 87545

Abstract
The Block IIA GPS satellites are equipped with a sensor designed to detect electromagnetic transients. Several phenomena will produce triggers in this sensor. They include earth-based electromagnetic transients such as lightning and two space-based phenomena – deep dielectric discharge and meteoroid or hyper-velocity micro-gram particle impact (HMPI). Energetic electrons in the GPS environment cause the deep dielectric charging. HMPIs cause triggers through the transient electric fields generated by the ejecta plasma. During the 1997 Leonid passage the energetic particle fluxes were very low. In the presence of such low fluxes the typical median trigger rate is 20 per minute with a standard deviation of about 20 per minute. Between 0800 UT and 1200 UT on November 17, 1997, the sensor on a specially configured satellite observed trigger rates more than 10 sigma above the nominal median rate. Sensors on other Block IIA GPS satellites also observed excess triggers during November. Detection is enhanced when the sensor antenna is oriented into the Leonid radiant. While many questions persist we feel that it is likely that the excess events during the November interval were caused by the close approach of the satellites to the Leonid meteoroid path.

1.0 Introduction

The GPS satellites' primary payload provides navigational information with global coverage. They have circular orbits about 4.1 R_e from the center of the earth. Orbital inclination is about 57 degrees. They have an orbital period of about 12 hours. The satellite orbits are arranged in six planes with four slots in each plane. In November 1997, seventeen Block IIA satellites were operational.

The GPS satellites include a secondary payload as well as the better known navigational payload. The secondary payload is the NDS (NUDET Detection System) payload. Elements of the NDS payload may include the BDD, BDY and W-Sensor Receiver/Processor (WSRP) sensors and the BDP processor. The BDD measures fluxes of energetic (> 250 keV) electrons and protons in the environment surrounding the satellite. When triggered the BDY measures the power-time profile of optical transients. When triggered the WSRP measures the power-time profile of electro-magnetic wave transients. The BDP controls the sensors and reads data from the sensors and passes it to the spacecraft for telemetry to the ground. The BDP reads both State of Health (SOH) and event data (*epro*) from the sensors.

2.0 WSRP Operation

2.1 Sensor Description

The WSRP consists of electromagnetic (EM) wave antennas, RF receivers and a processor. The WSRP monitors the VHF EM spectrum in two bands separated by the FM broadcast band. In each band the WSRP has three RF receivers preceded by narrow band filters or channels. The processor consists of trigger and timing circuitry. The processor generates an RMS average of the RF power in each channel. When the instantaneous RF power exceeds the RMS by a threshold offset value, the processor generates a channel alarm. When two of three channels in either band generate alarms within a temporal concurrence window, the processor generates a WSRP trigger. The processor then transmits a trigger flag and timing information to the BDP.

2.2 Sensor Response

Several phenomena will produce WSRP triggers. The two of three alarm and concurrence window requirements mean that the phenomena must generate energy over a wide frequency range within a short time span. Earth-based natural sources such as lightning can produce WSRP triggers. Data from the recently launched, DOE-sponsored FORTE (Fast On-board Recording of Transient Events) satellite confirms that earth-based sources can be identified by the dispersed nature of the trigger, i.e., the ionospheric plasma affects EM wave propagation causing the higher frequency components to reach the satellite before lower frequency components. Unfortunately, this technology was not available for the Block IIA WSRP sensors.

Some WSRP events are undispersed meaning that the signals are generated on or near the satellite. We have identified two mechanisms for generating undispersed triggers. Occasionally a hyper-velocity micro-gram particle impact (HMPI) will produce both an optical and an RF trigger. Laboratory tests have confirmed that this mechanism can produce optical triggers when the particle strikes the BDY sunshade and the ejecta leads to the generation of a transient optical signal. Apparently charged ejecta generate the RF signal directly or by a transient disruption of the sheath electric fields surrounding the spacecraft. HMPI's not striking the sunshade can probably generate RF triggers without generating optical triggers.

Laboratory experiments at Sandia (Crawford, 1997) have demonstrated that HMPIs can produce a dusty plasma and transient field and current fluctuations. Because the HMPIs produce oscillating electrical signals, it is possible that each HMPI produces several WSRP triggers. The WSRP response to HMPI effects provides no information about the mass, size or speed of the HMPI.

We have also identified a positive correlation between the energetic electron and proton fluxes and the WSRP trigger rate. We ascribe these triggers to deep dielectric discharge. We believe that deep dielectric discharge accounts for most of the WSRP triggers. Deep dielectric discharge does not produce an optical trigger.

2.3 On-board Data Processing and Telemetry

In the normal configuration the BDP does not transmit WSRP triggers if they are not coincident with optical triggers. The BDP does increment a counter, the *wevtct* (W event count), whenever it gets a WSRP trigger. If there is not a coincident optical trigger, the BDP increments another counter, the *wfaLct* (W false event count). At pre-set intervals, the *shint* (SOH interval), the BDP records the RMS noise levels in the six WSRP channels and queues these parameters and the counter values for transmittal in the SOH

data. It is important to emphasize that none of the data in this paper came from valid, simultaneous BDY and WSRP events. All data comes from State-of-Health (SOH) records.

2.4 Ground-based WSRP Data Processing

WSRP trigger rates can be derived from the SOH data by differencing the counter values and dividing by the SOH time interval. Normally the SOH interval is 60 minutes. The WSRP trigger rate is an average over the interval between SOH counter samples. Two rates can be associated with each SOH sample, either the average rate over the preceding interval or the average rate over the succeeding interval. Figure 1 shows the SVN 33 trigger rate versus time during an interval in September 1997, when the energetic particle flux was low. Typical trigger rates are 20 triggers per minute.

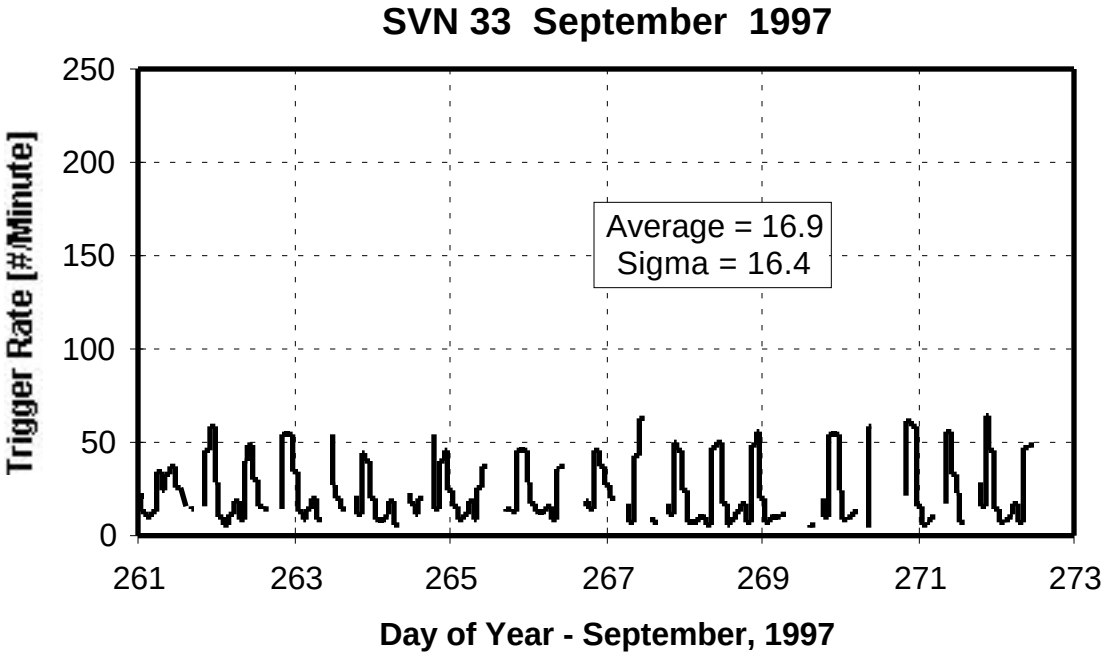

Figure 1. SVN 33 trigger rate versus time during an interval in September 1997, when the energetic particle flux was low. Note that peak rates rarely exceed 50/minute.

We have calculated multiple linear regressions correlating the WSRP trigger rate (dependent variable) with the RMS power levels in the six channels (six independent variables). We find an inverse correlation between the RMS power and the trigger rate (see Figure 2 for a plot of the trigger rate versus the RMS power in the High Band Mid Channel). The best fit line in Figure 2 comes from a single independent variable regression. Frequently, when the RMS power is low, the trigger rate is high and vice-versa. We hypothesize that the deep dielectric discharges are very weak, and when the RMS power is high, the trigger threshold is too high to allow deep dielectric discharges to cause channel alarms. The regression technique allows us to determine the effect of changing RMS power levels (and thereby changing trigger thresholds) upon the WSRP trigger rate. We can also subtract the regression predictions from the observed rates and study the residuals. We find that the residuals are frequently explained by changes in the energetic outer Van Allen belt electron fluxes. When the electron fluxes are relatively constant, as during the Leonid period in November 1997, we must find another mechanism, perhaps HMPIs, to explain the residuals.

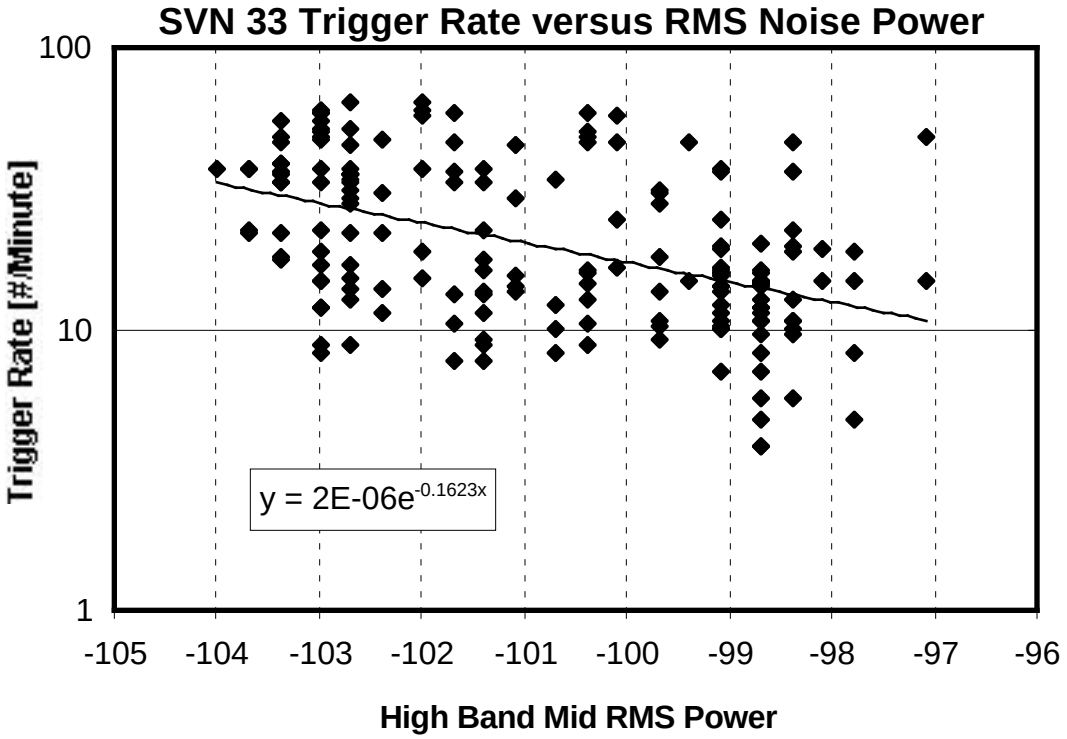

Figure 2. SVN 33 trigger rate versus the RMS power in the High Band Mid Channel for days 314 to 320, just prior to the Leonid encounter.

3.0 Energetic Particle Environment

The BDD on SVN 33 monitored the energetic, Van Allen belt radiation environment during 1997. Fluxes in the LE1 channel (~ 250 keV electrons) are most highly correlated with WSRP trigger rates. We have the capability of including all eleven BDD energetic particle channels as well as the six RMS noise channels in the multiple regression. Because of the low energetic particle background during the November 1997, Leonid interval we did not need this more complex regression. Instead, we identified 12 day intervals during preceding months when the energetic particle fluxes were the lowest, corresponding to the low levels surrounding November 17, 1997, days 314 to 326. For August the interval is days 213 to 225. For September the interval is days 261 to 273. For October the interval is days 287 to 299. The radiation belt fluxes were most similar to the Leonid interval during the September interval shown in Figure 1.

4.0 Leonid-related Observations

Figure 3 shows the WSRP trigger rates for SVN 33 from November 10 through November 22, including the Leonid interval. The contrast between event rates for the September and the November intervals is quite striking. Also note the high trigger rates on November 17, 1997, (day 321) during the peak Leonid interval. The peak rate of 220 per minute on November 17 is 12 sigma's above the September median rate! It is also significantly higher than the peak rates in the immediately preceding 6 days from days 314 to 320.

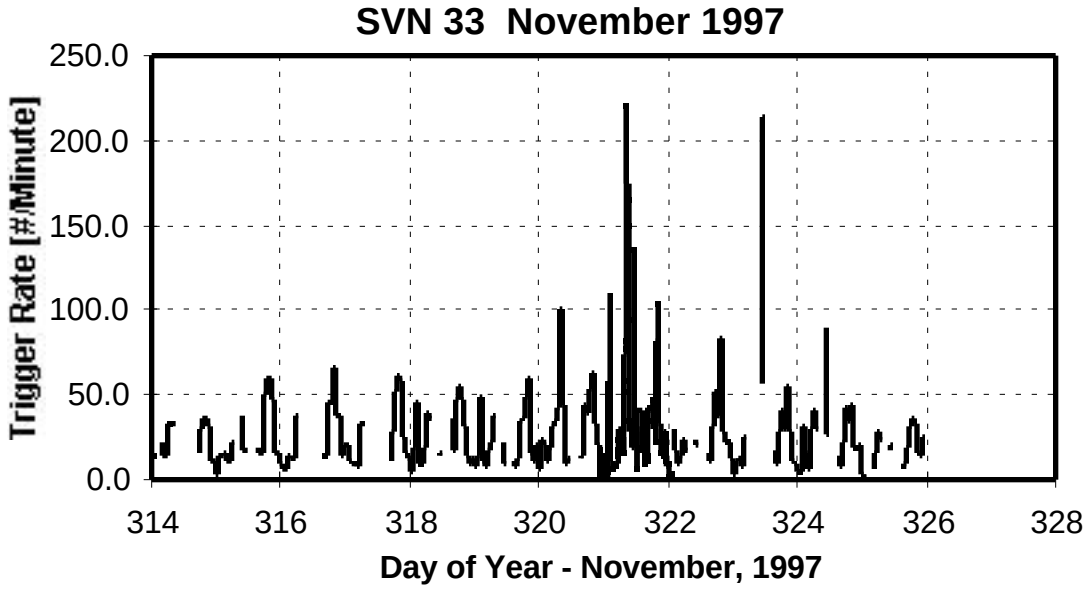

Figure 3. WSRP trigger rates for SVN 33 from November 10 through November 22, including the Leonid interval. Some rates on day 321 are many sigma above nominal.

The trigger rate depends upon the orientation of the satellite with respect to the Leonid radiant. Sensors on some satellites did not show evidence of HMPIs. Figure 4 shows the SVN 33 trigger rate and the angle, gamma, between the satellite orientation (the WSRP antenna always faces the earth) and the Leonid radiant as a function of time for days 320 through 325. The high trigger rates coincide with times when the WSRP antenna is facing into the Leonid radiant. Note the high rate just before noon on day 323, November 19, when the satellite is again facing into the Leonid radiant. The apparent HMPI effects are not limited to day 321, November 17.

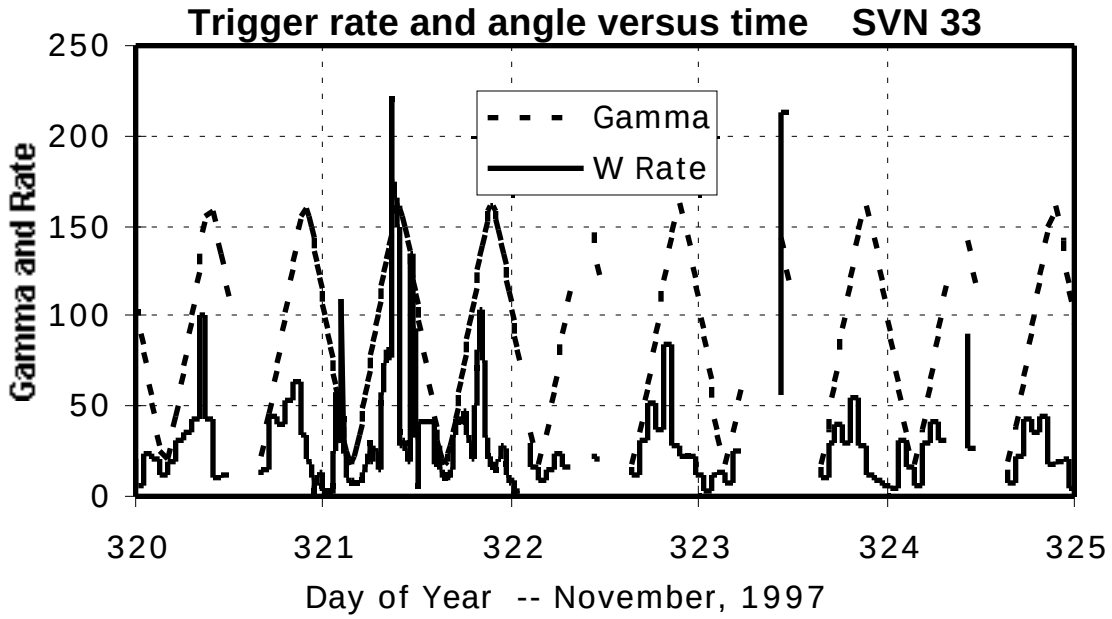

Figure 4. SVN 33 trigger rate and gamma, the angle between the satellite orientation and the Leonid radiant as a function of time for days 320 through 325. The high rates correspond to times when the antenna was facing the Leonid radiant.

Figure 5 shows the WSRP trigger rate from another satellite, SVN 23, as a function of gamma, the angle between the Leonid radiant and the WSRP antenna pointing for the November interval. The highest trigger rates occur when the satellite is pointed closest to the Leonid radiant. Several times the trigger rate exceeds 200 per minute! Because the WSRP may detect several electric field oscillations per HMPI we caution against assuming that 200 HMPIs strike the WSRP antenna, or even the front face of the satellite, per minute.

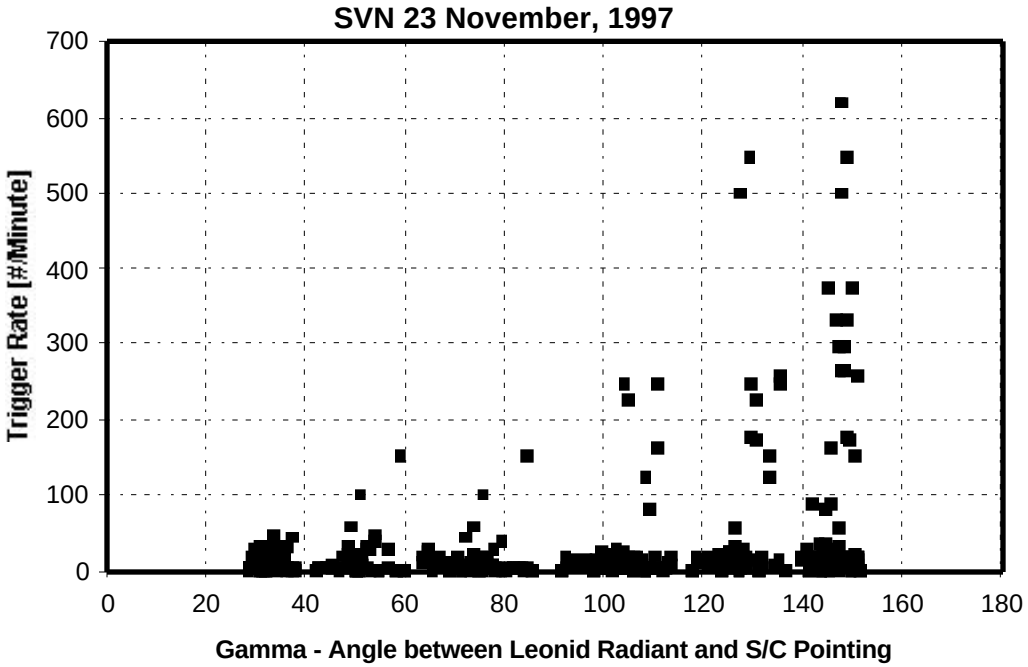

Figure 5. SVN 23 WSRP trigger rate as a function of gamma, the angle between the Leonid radiant and the WSRP antenna pointing for the November interval. The highest rates correspond to time when the satellite was facing the Leonid radiant.

Figure 6 shows the WSRP trigger rate as a function of pointing for the September interval. The observed rate is essentially independent of satellite orientation during this time.

5.0 **Conclusions and Recommendations**

We know that the WSRP is sensitive to HMPI's. Clearly the mid-November WSRP event rates were quite unusual. High WSRP rates required satellite pointing into the Leonid radiant. While many questions persist we feel that it is likely that the excess WSRP events during the November interval were caused by the close approach of earth to the Leonid meteor path.

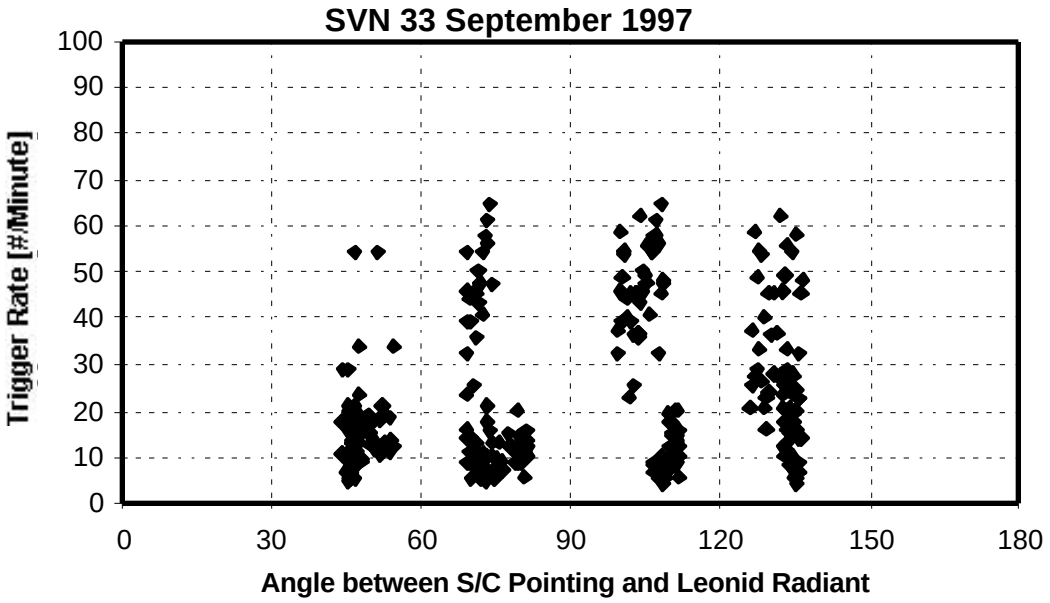

Figure 6. WSRP trigger rate as a function of pointing for the September interval.

We recommend further study including examination of event rates for W-Sensors on GPS satellites during previous meteor showers, including the Perseids. We also recommend de-coupling the BDY and WSRP sensor on selected satellites during the upcoming Perseid and Leonid showers.

References:

"The Production of Plasma and Consequent Electrostatic and Magnetic Fields During Hypervelocity Impacts," David Crawford, presented to Leonid Meteor Storm Conference, April 8-9, 1997.